Structure, spectroscopic and electronic properties of a well defined silica supported olefin metathesis catalyst, [(≡SiO)Re(≡CR)(=CHR)(CH_2R)], through DFT periodic calculations: silica is just a large siloxy ligand†

Xavier Solans-Monfort,[a] Jean-Sébastien Filhol,[a] Christophe Copéret*[b] and Odile Eisenstein*[a]

Received (in Montpellier, France) 7th March 2006, Accepted 30th March 2006
First published as an Advance Article on the web 5th May 2006
DOI: 10.1039/b603426h

DFT plane-wave periodic calculations using the VASP code have been carried out to model the silica supported olefin metathesis catalyst, [(≡SiO)Re(≡CR)(=CHR)(CH_2R)]. The structure, spectroscopic and electronic properties of this highly active catalyst have been compared with those of non-efficient molecular analogues, [(X_3SiO)Re(≡CR)(=CHR)(CH_2R)] (X_3SiO is triphenylsiloxy or polyoligomeric silsesquioxane (POSS)). The silica surface was modelled using cristobalite and edingtonite ideal polymorph surfaces, and the organometallic fragment has been represented with the experimental (R = *t*Bu) and simplified (R = Me) ligands, [(≡SiO)Re(≡CR)(=CHR)(CH_2R)]. The calculated structures, alkylidene J_{C-H} coupling constants and ν_{C-H} stretching frequencies agree with experimental data. The *syn* and *anti* isomers of the Re complexes are close in energy, the former being always more stable. A secondary Re···O interaction experimentally detected by EXAFS is found to have no stabilizing influence, but is possible because of the facile distortion of (≡SiO)Re(≡CR)(=CHR)(CH_2R). More importantly, the geometry and electronic structure of the Re fragment is essentially the same for the triphenylsiloxy, the POSS and the silica surface, which shows that the siloxy group of the first coordination sphere of Re determines the metal properties. The silica surface is thus electronically equivalent to the other siloxy groups, and should be viewed as a large bulky ligand.

Introduction

Olefin metathesis was discovered by using catalysts based on transition metal oxides supported on oxide surfaces.[1] In particular, one of the most efficient catalysts, able to work at room temperature, is Re_2O_7/Al_2O_3.[2] However, difficulty in characterizing the active site has probably impaired its development into a commercial process. In contrast, the proposal of Chauvin, where metallocarbenes are key intermediates,[3,4] led to the preparation of a large number of well-defined and efficient homogeneous catalysts based on early (Mo, W and Re)[5,6] and late transition metals[7–9] (Ru) through the powerful tools of molecular organometallic chemistry. By combining the advantages of homogenous and heterogeneous catalysis, surface organometallic chemistry uses a molecular approach to construct well-defined active sites for heterogeneous catalysts.[10] Applying this strategy to olefin metathesis[11] led to the development of a well-defined silica-supported alkylidene Re complex, [(≡SiO)Re(≡C*t*Bu)(=CH*t*Bu)(CH_2*t*Bu)] (**1**), which shows unprecedented activity in olefin metathesis compared to both homogeneous and heterogeneous Re-based catalysts.[11–13]

The silica supported catalyst, [(≡SiO)Re(≡C*t*Bu)(=CH*t*Bu)(CH_2*t*Bu)] (**1**), is prepared by reaction of [Re(≡C*t*Bu)(=CH*t*Bu)(CH_2*t*Bu)$_2$] with a silica partially dehydroxylated at 700 °C (Scheme 1) and has been characterized by IR, solid state NMR and EXAFS spectroscopies.[13–15] No residual silanol group is detected after grafting of the metal complex. These experimental techniques allow the characterization of the chemical identity of the catalyst but do not provide detailed geometrical information on the grafted

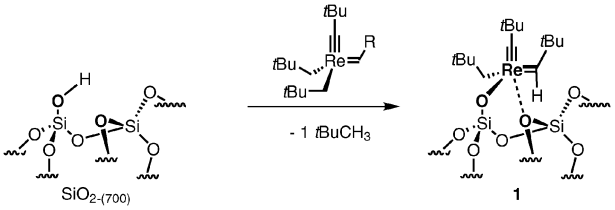

Scheme 1

[a] *LSDSMS (UMR 5636-CNRS-UM2), Institut Gerhardt, Université Montpellier 2, F-34095 Montpellier Cedex 05, France. E-mail: odile.eisenstein@univ-montp2.fr; Fax: +33 0467144839; Tel: +33 0467143306*
[b] *LCOMS, (UMR 9986 CNRS-CPE Lyon), CPE Lyon, 43 Bd du 11 Novembre 1918, F-69616 Villeurbanne Cedex, France. E-mail: coperet@cpe.fr; Fax: +33 0472431795; Tel: +33 0472431811*

† Electronic Supplementary Information (ESI) available: Table S1 gives the syn/anti relative energies and several geometrical parameters of Re(≡CCH$_3$)(=CHCH$_3$)(CH_2CH$_3$)(OSiH$_3$) (**1M$_q$**) and Re(≡CCH$_3$)(=CHCH$_3$)(CH_2CH$_3$)$_2$ (**2M$_q$**) systems for B3PW91 or PBEPBE density functionals. Figs. S1, S2, and S3 give the optimized geometries of the full systems **1M$_f$**, **E$_{(100)}$-1$_f$**, and **1P$_f$** respectively. Fig. S4 gives the band decomposed charge density for the three highest occupied bands. See DOI: 10.1039/b603426h

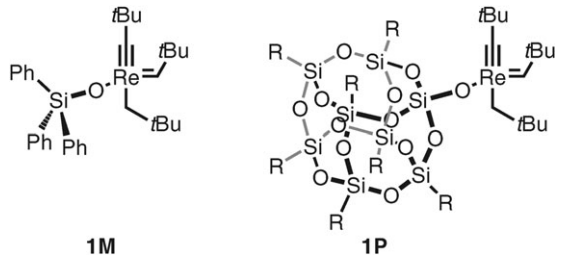

1M 1P

Scheme 2

fragment. Thus, the structures are assigned *via* comparison with the corresponding homologous molecular complexes, $[(R_3SiO)Re(\equiv CtBu)(=CHtBu)(CH_2tBu)]$, which have been fully synthesized and characterized (**1M** and **1P** in Scheme 2).[13,14,16] These complexes have a pseudo-tetrahedral geometry with coplanar alkylidene and alkylidyne ligands, and they are present as 10 : 1 mixtures of *syn* and *anti* isomers.[16] It is noteworthy that the J_{C-H} coupling constant for the alkylidene proton is much lower for the *syn* (116 Hz) than for the *anti* isomer (159 Hz); the low coupling constant for the *syn* isomer has been associated with an elongated C–H bond and the presence of an α-agostic interaction.[17,18] In the case of the silica supported complexes, the resemblance in the spectroscopic properties with molecular homologues suggests similar chemical entities. A *syn* isomer with J_{C-H} equal to 109 Hz is formed selectively during grafting, and it is partially interconverted into an *anti* isomer with J_{C-H} equal to 159 Hz upon heating at 120 °C. EXAFS spectroscopy suggests the presence of a weak secondary interaction between the rhenium center and an oxygen atom of the silica surface with a Re···O distance of 2.42 Å. In spite of similar features between homogeneous and silica grafted complexes, the reactivity in olefin metathesis of **1M**, **1P** and **1** is very different, **1** being the only efficient catalyst. It is thus of importance to determine to what extent the surface modifies the structure and electronic properties of the metal fragment.

While molecular organometallic complexes are calculated by DFT methods with good accuracy at relatively low CPU times,[19] the modeling of heterogeneous catalysts based on amorphous supports is still a challenge for computational chemists, because of the complexity of amorphous systems and the associated costly calculations. Computational modeling of amorphous solids was performed using three approximations: clusters, embedded clusters and periodic solids, the latter being usually considered as the most accurate approach. In the particular case of amorphous silica, the periodic models are constructed from an ideal polymorph of SiO_2, in particular α-quartz,[20] β-cristobalite[20–24] and edingtonite.[25–28] Transition metal based catalysts on silica surfaces have been modeled using finite clusters[29–42] and CPMD calculations have been carried out for a silica supported zirconium hydride.[22] In this work, we have carried out DFT periodic calculations of the experimental organometallic silica grafted complexes including the real set of ligands. For the present systems, the large available experimental data (*syn*/*anti* ratio, EXAFS, IR and NMR spectroscopies) on the molecular (**1M** and **1P**) and the grafted Re complexes (**1**) allows us to test our periodic models and to compare homogeneous and surface complexes.

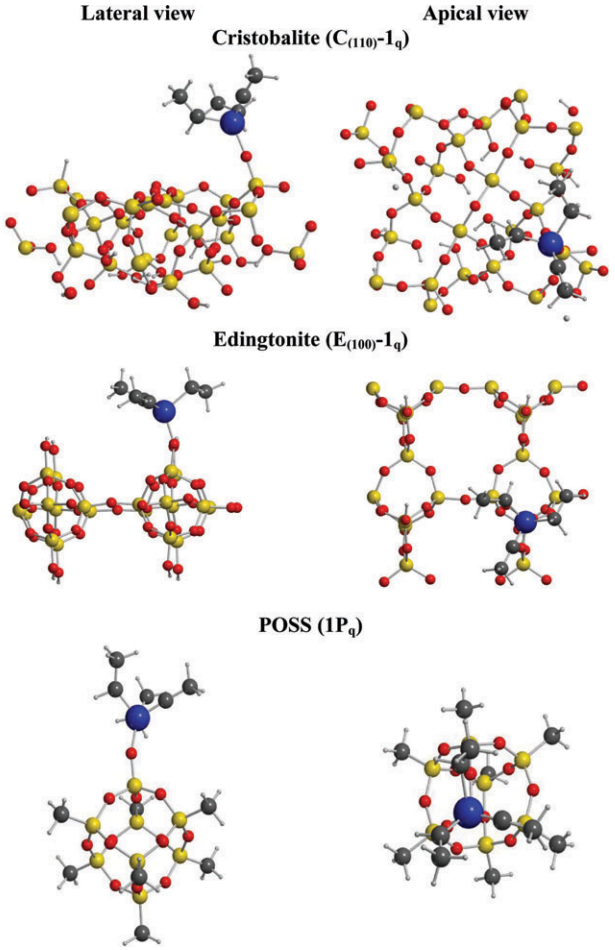

Fig. 1 Silica surface ($\mathbf{C_{(110)}}$-$\mathbf{1_q}$ and $\mathbf{E_{(100)}}$-$\mathbf{1_q}$) and POSS ($\mathbf{1P_q}$) models.

Models and computational details

Models

The silica surface has been modeled by cristobalite ($\mathbf{C_{(110)}}$),[21–24] and edingtonite ($\mathbf{E_{(100)}}$),[25–27] which are both represented in Fig. 1. $\mathbf{C_{(110)}}$ is constructed by cutting β-cristobalite parallel to the (110) face because it is the only face where dehydroxylation can be represented by elimination of H_2O and formation of Si–O–Si bridges with limited geometrical constraints. The thickness of the slab is around 6 Å, and the vacuum between the slabs is set to about 19 Å. The surfaces are terminated by oxygen atoms, which are saturated with hydrogen atoms forming a hydroxyl group, and 2 × 2 supercells are constructed. The constructed surfaces have 4 hydroxyl groups: one is substituted by the Re fragment, two are dehydrated by removing a water molecule and forming one new Si–O–Si bridge and finally the last one is replaced by a H. This latter termination is used because it is less reactive than a hydroxyl and far from the Re center (7.5 Å in the optimized structures). This model represents the experimental surface where no silanol is found after grafting. The $\mathbf{C_{(110)}}$ cell without the grafted metal species contains 106 atoms.

The $\mathbf{E_{(110)}}$ model is constructed by cutting the edingtonite bulk parallel to the (100) face. The surface is terminated by hydroxyl groups, and the final unit cell includes 4 (2 × 2) Y

edingtonite building blocks of formula $(SiO_2)_5$ (see Fig. 1). The constructed surfaces have 4 hydroxyl groups: one is substituted by the Re fragment and the three others are left untouched because of the rigidity of the framework, which prevents their interaction with the grafted complex. The vacuum between two slabs is fixed to about 19 Å. The $\mathbf{E_{(110)}}$ cell without the grafted metal species includes 78 atoms.

Two representations of the grafted model are considered (Scheme 3): a simplified (small) model $\mathbf{1_q}$, in which the *t*Bu are replaced by methyl groups, [(≡SiO)Re(≡CCH$_3$)(=CHCH$_3$)(CH$_2$CH$_3$)], and the full system $\mathbf{1_f}$ [(≡SiO)Re(≡C*t*Bu)(=CH*t*Bu)(CH$_2$*t*Bu)] in which the experimental ligands are used. The cristobalite and edingtonite supported systems are labeled as $\mathbf{C_{(110)}}$-**1** and $\mathbf{E_{(110)}}$-**1**, where **1** is replaced by $\mathbf{1_q}$ and $\mathbf{1_f}$ to represent the small and the full systems, respectively. For example, the *syn* isomer of the small and full systems grafted on cristobalite (110) surface are called hereafter *syn*-$\mathbf{C_{(110)}}$-$\mathbf{1_q}$ and *syn*-$\mathbf{C_{(110)}}$-$\mathbf{1_f}$, respectively. The separation between the closest ligands of two equivalent grafted complexes is around 6.5 Å for the small system and 4.5 Å for the full system, which does not induce significant interaction between alkyl substituents of two rhenium fragments on different unit cells.

The unit cell parameters are allowed to relax initially for *syn*-$\mathbf{C_{(110)}}$-$\mathbf{1_q}$ and *syn*-$\mathbf{E_{(100)}}$-$\mathbf{1_q}$ until the total pressure is lower than 10 kbar to remove the overestimated stress associated with the dehydration in this relatively small unit cell. The *a* and *b* cell parameters contract by an average of 7% upon optimization. The final inter Re distance is equal to the experimental 13 Å average distance. The same unit cell parameters are used for all the other systems. All atom positions are allowed to relax except for the terminal OH groups of the bottom $\mathbf{C_{(110)}}$ face, which are not relevant and can cause small artificial energy fluctuations.

The molecular analogues are computed as a periodic array of isolated molecular systems (Scheme 3 and Fig. 1). For **1M**, [Ph$_3$SiO–Re(≡C*t*Bu)(=CH*t*Bu)(CH$_2$*t*Bu)], the small and full calculated models are $\mathbf{1M_q}$, [H$_3$SiO–Re(≡CMe)(=CHMe)(CH$_2$Me)], and $\mathbf{1M_f}$ [Ph$_3$SiO–Re(≡C*t*Bu)(=CH*t*Bu)(CH$_2$*t*Bu)], respectively. For [(*c*-C$_5$H$_9$)$_7$Si$_7$O$_{12}$SiO–Re(≡C*t*Bu)(=CH*t*Bu)(CH$_2$*t*Bu)] **1P**, the small and full models are $\mathbf{1P_q}$, [(Me)$_7$Si$_7$O$_{12}$SiO–Re(≡CMe)(=CHMe)(CH$_2$Me)], and $\mathbf{1P_f}$ [(Me)$_7$Si$_7$O$_{12}$SiO–Re(≡C*t*Bu)(=CH*t*Bu)(CH$_2$*t*Bu)], respectively. Test calculations have shown that the replacement of the cyclopentyl by methyl substituents in **1P** give similar results. These molecular species are included in a 22 Å length cubic unit cell. This unit cell is not allowed to relax, and it leads to separations between the complexes that are larger than 9 Å for the largest system $\mathbf{1P_f}$. These separations are sufficient to avoid interactions between periodic images.

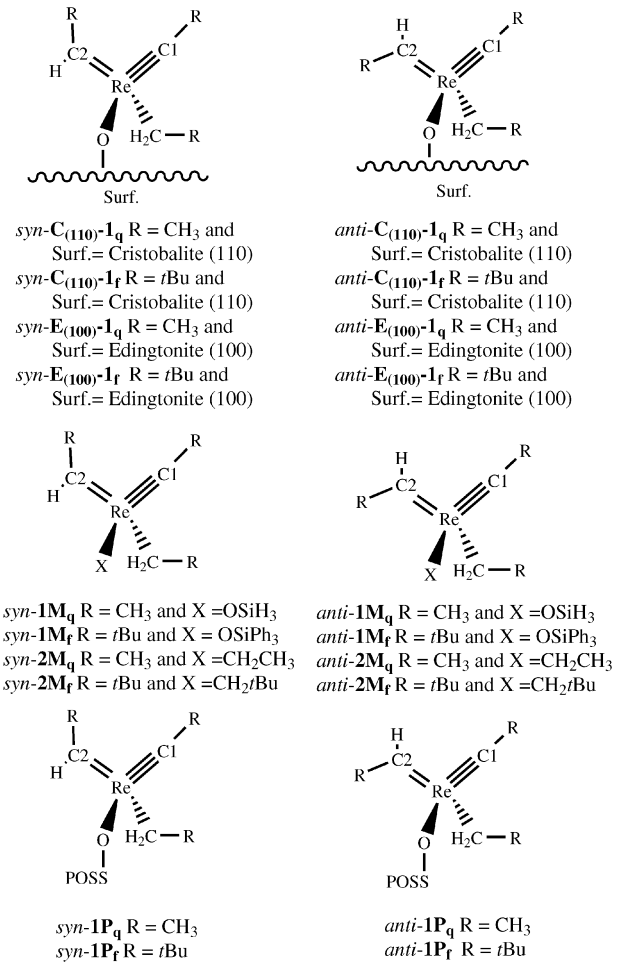

syn-$\mathbf{C_{(110)}}$-$\mathbf{1_q}$ R = CH$_3$ and Surf.= Cristobalite (110)
syn-$\mathbf{C_{(110)}}$-$\mathbf{1_f}$ R = *t*Bu and Surf.= Cristobalite (110)
syn-$\mathbf{E_{(100)}}$-$\mathbf{1_q}$ R = CH$_3$ and Surf.= Edingtonite (100)
syn-$\mathbf{E_{(100)}}$-$\mathbf{1_f}$ R = *t*Bu and Surf.= Edingtonite (100)

anti-$\mathbf{C_{(110)}}$-$\mathbf{1_q}$ R = CH$_3$ and Surf.= Cristobalite (110)
anti-$\mathbf{C_{(110)}}$-$\mathbf{1_f}$ R = *t*Bu and Surf.= Cristobalite (110)
anti-$\mathbf{E_{(100)}}$-$\mathbf{1_q}$ R = CH$_3$ and Surf.= Edingtonite (100)
anti-$\mathbf{E_{(100)}}$-$\mathbf{1_f}$ R = *t*Bu and Surf.= Edingtonite (100)

syn-$\mathbf{1M_q}$ R = CH$_3$ and X =OSiH$_3$
syn-$\mathbf{1M_f}$ R = *t*Bu and X = OSiPh$_3$
syn-$\mathbf{2M_q}$ R = CH$_3$ and X =CH$_2$CH$_3$
syn-$\mathbf{2M_f}$ R = *t*Bu and X =CH$_2$*t*Bu

anti-$\mathbf{1M_q}$ R = CH$_3$ and X =OSiH$_3$
anti-$\mathbf{1M_f}$ R = *t*Bu and X = OSiPh$_3$
anti-$\mathbf{2M_q}$ R = CH$_3$ and X =CH$_2$CH$_3$
anti-$\mathbf{2M_f}$ R = *t*Bu and X =CH$_2$*t*Bu

syn-$\mathbf{1P_q}$ R = CH$_3$
syn-$\mathbf{1P_f}$ R = *t*Bu

anti-$\mathbf{1P_q}$ R = CH$_3$
anti-$\mathbf{1P_f}$ R = *t*Bu

Scheme 3 *syn* (left) and *anti* (right) isomers of all studied species.

Level of theory

Geometry optimizations of all systems have been performed using periodic density functional theory (DFT) calculations within the projector augmented-wave (PAW) formalism[43,44] as implemented in the VASP package.[45,46] The exchange–correlation energy and potential are described by the PBEPBE functional.[47] We have used Monkhorst–Pack[48] sampling of the Brillouin zone with a (2,2,1) mesh for the surface calculations and a gamma mesh for the molecular ones.[48] The plane wave cut-off has been fixed to 400 eV. The convergence with the number of *k*-points and with the basis set has been tested in the $\mathbf{C_{(110)}}$-$\mathbf{1_q}$ model by performing two sets of single point calculations increasing the number of *k*-points up to a (6,6,1) grid, and the cut-off up to 700 eV. In both cases no significant difference in the *syn*/*anti* relative energies is obtained enabling the lower level to be selected. Convergence is obtained when the maximum force on all atoms was <0.01 eV Å^{-1}.

In our previous work,[16] we have performed molecular calculations of Re(≡CR)(=CHR)(X)(Y) complexes using the GAUSSIAN03 package[49] with the B3PW91 functional. The Re and Si atoms were represented by the quasi-relativistic effective core pseudo-potentials (RECP) of the Stuttgart group, and the associated basis sets augmented with a polarization function.[50–53] The C, O and H atoms were represented by the 6-31G(d,p) basis set.[54] In order to verify that the nature of the functional has no influence on the structure, the *syn*/*anti* relative energies (ΔE) and the spectroscopic properties (ν_{C-H}, J_{C-H}), we repeated the calculations on Re(≡CR)(=CHR)(CH$_2$R)(OSiR′$_3$) (R = CH$_3$ R′ = H, $\mathbf{1M_q}$, R = *t*Bu, R′ = Ph, $\mathbf{1M_f}$) and Re(≡CR)(=CHR)(CH$_2$R)$_2$ (R = CH$_3$, $\mathbf{2M_q}$; R = *t*Bu, $\mathbf{2M_f}$) with the PBEPBE functional without changing the basis sets and RECP (Table S1†). Geometries, ΔE, ν_{C-H} and J_{C-H} are found to be identical with the two functionals.

In addition, the influence of the ligands on the geometries and spectroscopic properties of the complexes is also reproduced in a similar manner with the two functionals. Finally, Gaussian (PBE) and VASP (PBE) calculations lead also to equivalent results indicating that the 22 Å length cubic unit cell for the periodic calculation properly represents an isolated molecule (Fig. 2, Fig. S1 and Table 1). The only geometry difference is found for the very soft Re–O–Si angle (see later). Optimization with an extended basis set (6-311+G*) on the oxygen atom led to better agreement (Re–O–Si = 152°)

The C_{ene}–H_{α} vibrational frequencies (ν_{C-H}) have been calculated numerically for the systems computed with VASP. Since the C–H stretching frequency has been previously identified as an isolated mode,[16] the calculations were restrained to C_{ene} and H_{α} atoms. In the case of molecular species calculated with GAUSSIAN03, the C_{ene}–H_{α} vibrational frequencies are computed analytically assuming a harmonic approach. NMR C_{ene}–H_{α} coupling constants (J_{C-H}) have been computed with GAUSSIAN03 package with IGLOII basis sets[55,56] only for the small model because these calculations are highly time consuming. In the case of the large **1P$_q$**, **C$_{(110)}$-1$_q$** and **E$_{(100)}$-1$_q$** systems, the J_{C-H} coupling constant is computed considering only a finite cluster of the whole optimized structures (see below).

Results and discussion

The silica supported [(≡SiO)Re(≡CtBu)(=CHtBu)(CH$_2$tBu)] complex

The optimized geometries of the *syn* and *anti* isomers of the [(≡SiO)Re(≡CR)(=CHR)(CH$_2$R)] complex grafted on cristobalite (110) using the small **C$_{(110)}$-1$_q$** and full **C$_{(110)}$-1$_f$** models are represented in Fig. 3, and Table 2 summarizes the *syn*/*anti* relative energies and selected spectroscopic values for these systems. The complexes grafted onto cristobalite have a pseudo-tetrahedral geometry with a small angle between the alkylidene and alkylidyne ligands (between 95 and 100°). The calculated bond lengths for the four different ligands are different as expected, while they were previously obtained by EXAFS as the average values for the multiple (M≡C and M=C) and single (M–C and M–O) bonds.[14] The alkylidene and alkylidyne ligands are co-planar, which gives rise to *syn* and *anti* isomers. For the *syn* isomer, the Re–C–H angle is 106.1°, and the C–H bond length is 1.116 Å. For the *anti* isomer, the corresponding values are 126.6° and 1.096 Å. These geometry parameters are indicative of the existence of a C–H α-agostic interaction in the *syn* isomer only. In the two isomers, the Re–O–Si angle is close to 180°, and the ligands are far from the silica surface. Introducing the full ligand set in the calculation, **C$_{(110)}$-1$_f$**, does not modify the coordination around Re and does not change the orientation of the metal fragment with respect to the surface (Fig. 3). The most stable conformers of *syn*- and *anti*-**C$_{(110)}$-1$_f$** are those in which the *t*Bu group of the neopentyl ligand is staggered with respect to the other ligands around Re and avoids as much as possible the *t*Bu groups of the alkylidene or alkylidyne ligands as illustrated by the Newman projections along the Re–C_{alkyl} bond in Scheme 4. Therefore, the *t*Bu group of the neopentyl ligand

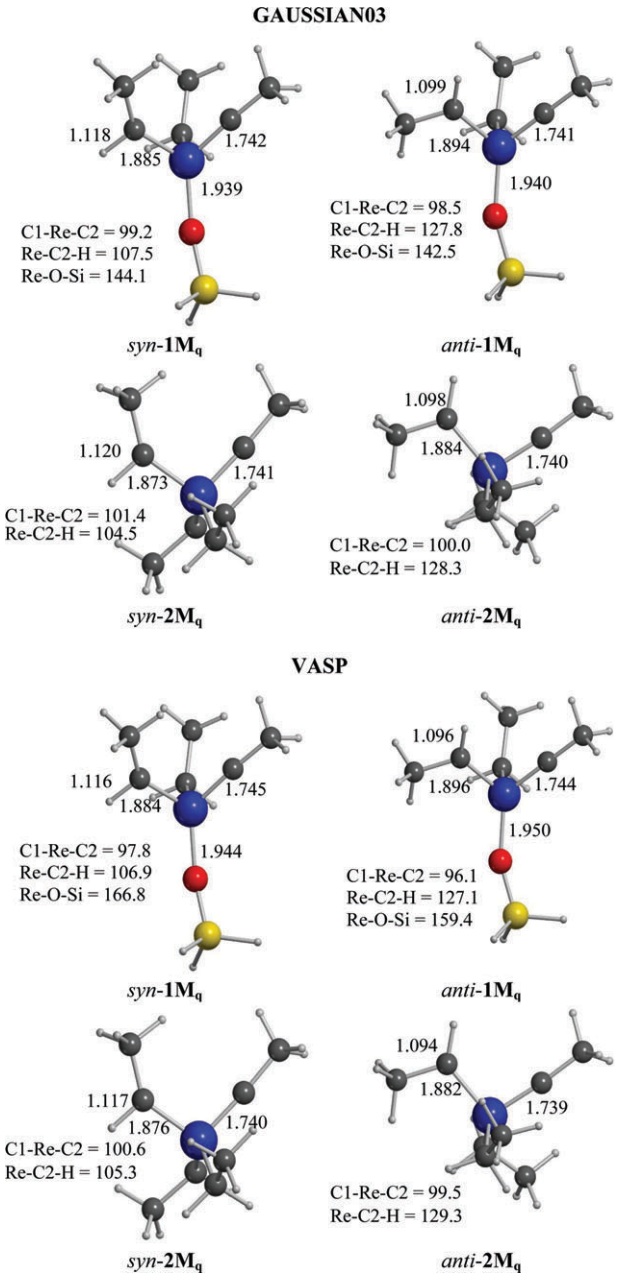

Fig. 2 Optimized structures of Re(≡CCH$_3$)(=CHCH$_3$)(CH$_2$CH$_3$)(OSiH$_3$) (**1M$_q$**) and Re(≡CCH$_3$)(=CHCH$_3$)(CH$_2$CH$_3$)$_2$ (**2M$_q$**) using GAUSSIAN and VASP methodologies. See Scheme 3 for atom labelling. Distances in Å and angles in degrees.

is *gauche* to the alkylidene group in *syn*-**C$_{(110)}$-1$_f$**, but *gauche* to the alkylidyne group in *anti*-**C$_{(110)}$-1$_f$**.

The *syn* **C$_{(110)}$-1$_q$** is 2.2 kcal mol^{-1} more stable than the *anti* **C$_{(110)}$-1$_q$** (Table 2). When the full system is considered, the difference between the *syn* and *anti* isomers is reduced to 1.5 kcal mol^{-1}. Although these energy differences are small, they reproduce the experimental preference for the *syn* isomer, and the fact that both isomers can be detected. Such agreement could appear fortuitous, but it is well known that similar remarkable agreement between experimental and computation can be obtained when comparing isomers of large organometallic complexes.[16,57,58]

Table 1 Relative energies in kcal mol^{-1}, stretching frequencies (ν_{C-H}) in cm^{-1} and NMR coupling constants (J_{C-H}) in Hz, for C2–H bonds for Re(≡CCH$_3$)(=CHCH$_3$)(CH$_2$CH$_3$)(OSiH$_3$) (**1M$_q$**), Re(≡CCH$_3$)(=CHCH$_3$)(CH$_2$CH$_3$)$_2$ (**2M$_q$**) and Re(≡C*t*Bu)(=CH*t*Bu)(CH$_2$*t*Bu)(OSiPh$_3$) (**1M$_f$**)

Structure[a]	ΔE(calc)/ kcal mol^{-1}	ΔE(exp)[b]/ kcal mol^{-1}	ν_{C-H} (calc)/ cm^{-1}	J_{C-H} (calc)/ cm^{-1}	J_{C-H} (exp)/ Hz
syn-**1M$_q$-G**[c]	0.0	0.0	2861	111	116
anti-**1M$_q$-G**[c]	1.1	1.4	3085	149	159
syn-**2M$_q$-G**[c]	0.0	0.0	2883	112	113
anti-**2M$_q$-G**[c]	2.1	1.4	3075	153	154
syn-**1M$_q$**	0.0	0.0	2878	110	116
anti-**1M$_q$**	1.2	1.4	3051	148	159
syn-**2M$_q$**	0.0	0.0	2874	113	113
anti-**2M$_q$**	2.5	1.4	3083	156	154
syn-**1M$_f$**	0.0	0.0	2879		116
anti-**1M$_f$**	1.0	1.4	3019		159

[a] See Fig. 2 and S1 (ESI). [b] Calculated from the *syn*/*anti* observed ratio. [c] Calculated as an isolated molecule with GAUSSIAN03 package.

The vibrational C$_{ene}$–H$_\alpha$ stretching frequency, ν_{C-H}, and the C$_{ene}$–H$_\alpha$ NMR coupling constants, J_{C-H}, have been calculated for **C$_{(110)}$-1$_q$** (Table 2). The calculations of NMR coupling constants for large systems are challenging[56,59–62] and in particular they cannot be carried out for periodic systems. Therefore, NMR coupling constants have been calculated with cluster models using the geometry obtained from periodic calculations. Because the size of the appropriate cluster cannot be determined *a priori*, we have varied their sizes as shown in Fig. 4, but the calculated J_{C-H} values are not affected by this factor. The calculated J_{C-H} values are also close to the experimental ones for both *syn* and *anti* isomers considering the accuracy of ±10 Hz[60,62] for DFT calculated NMR coupling constants (J_{calc} = 111 Hz compared J_{exp} = 109 Hz for the *syn* isomer and J_{calc} = 150 Hz compared to J_{exp} = 159 Hz for the *anti* isomer). Additionally, the alkylidene C–H bond of the *syn* isomer, which has a low J_{C-H} coupling constant, is also associated with a lower ν_{C-H} value (2879 for *syn*-**C$_{(110)}$-1$_q$** *vs.* 3063 cm^{-1} for *anti*-**C$_{(110)}$-1$_q$** and 2840 for *syn*-**C$_{(110)}$-1$_f$** *vs.* 3032 cm^{-1} for *anti*-**C$_{(110)}$-1$_f$**). This probably explains the presence of a broad band at low frequency in the C–H bond region of the experimental spectrum (2700–2800 cm^{-1}). Both data, low J_{C-H} and ν_{C-H}, are consistent with a weakened alkylidene C–H bond in the *syn* isomer, associated with the presence of a C–H α-agostic interaction.

Changing the silica model from cristobalite to edingtonite has little effect on the properties of the Re fragment (Fig. 5 and Fig. S2; Table 2). The main difference is the decrease of the Si–O–Re angle from 173.6° in *syn*-**C$_{(110)}$-1$_q$** to 157.1° in *syn*-**E$_{(100)}$-1$_q$**, which is associated with an increase between the *syn* and *anti* isomer energy difference from 2.2 to 3.0 kcal mol^{-1}, but which does not change the coordination properties around Re as evidenced by the calculated J_{C-H} and ν_{C-H}. It is worth mentioning that a change of the Re–O–Si angle from 130° to 175° modifies the total energy by no more than 1 kcal mol^{-1} showing considerable flexibility of the system through bending at the siloxy oxygen of the grafting group. The inclusion of the *t*Bu groups produces a similar behaviour to that described for the **C$_{(110)}$** model. In summary, the cristobalite and edingtonite models of the silica supported Re complex [(≡SiO)Re(≡C*t*Bu)(=CH*t*Bu)(CH$_2$*t*Bu)] give almost identical geometrical features, a slight energy preference for the *syn* isomer and similar spectroscopic information for the alkylidene C–H bond. In consequence, the structure of the silica surface has little influence on the coordination features of the Re fragment.

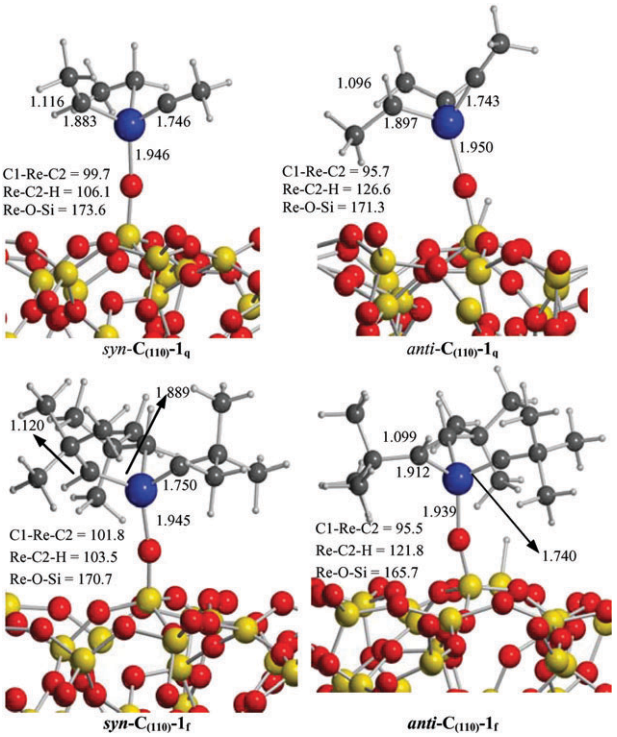

Fig. 3 Optimized structures of [(≡SiO)Re(≡CCH$_3$)(=CHCH$_3$)(CH$_2$CH$_3$)] using cristobalite as surface model (**C$_{(110)}$-1q**). See Scheme 3 for atom labelling. Distances in Å and angles in degrees.

The Re···O secondary interaction

The EXAFS measurements suggest the presence of a secondary Re···O interaction with a remote oxygen, leading to pentacoordinated rhenium.[14] This is consistent with the electron deficiency at Re in these complexes. We have first tested the ability of an oxygen of the silica surface to interact with the rhenium atom without the geometrical constraints associated with the model surface. This was modelled by setting a free SiH$_3$–O–SiH$_3$ at a distance of 2.4 Å from the rhenium species grafted on the cristobalite. After geometry optimization, the Re···O value is 2.7 Å, indicating that SiH$_3$–O–SiH$_3$ is within bonding distance of Re (Fig. 6). The rhenium complex distorts to form a SiH$_3$–O–SiH$_3$ adduct; this adduct has a trigonal bipyramidal geometry with apical disiloxy ether and ethyl group. The geometry of this adduct is thus similar to the ethylene adduct intermediate found on the reaction path of olefin metathesis with analogous homogeneous Re catalysts.[63] This coordination is athermic, showing that the Re···O interaction is weak, and that the rhenium complex is not really stabilized by this interaction. The J_{C-H} coupling constant for the alkylidene C–H bond, which has been found to be a highly sensitive reporter of the electronic properties of Re, was calculated to be 108 Hz for the disiloxy ether adduct, which only differs by 3 Hz from the value without disiloxy ether.

Table 2 Relative energies in kcal mol^{-1}, stretching frequencies (ν_{C-H}) in cm^{-1} and NMR coupling constants (J_{C-H}) in Hz for C2–H bonds for [(≡SiO)Re(≡CCH$_3$)(=CHCH$_3$)(CH$_2$CH$_3$)] (**1$_q$**) and [(≡SiO)Re(≡C*t*Bu)(=CH*t*Bu)(CH$_2$*t*Bu)] (**1$_f$**) using cristobalite (**C$_{(110)}$**) and edingtonite models (**E$_{(100)}$**)

Structure[a]	ΔE/ kcal mol^{-1}	ΔE(exp)[b]/ kcal mol^{-1}	ν_{C-H} (calc)/ cm^{-1}	J_{C-H} (calc)/ cm^{-1}	J_{C-H} (exp)/ Hz
syn-**C$_{(110)}$-1$_q$**	0.0	0.0	2879	111[c]	109
anti-**C$_{(110)}$-1$_q$**	2.2	0.5	3063	150[c]	159
syn-**C$_{(110)}$-1$_f$**	0.0	0.0	2840		109
anti-**C$_{(110)}$-1$_f$**	1.5	0.5	3032		159
syn-**E$_{(100)}$-1$_q$**	0.0	0.0	2875	111[c]	109
anti-**E$_{(100)}$-1$_q$**	3.0	0.5	3070	149[c]	159
syn-**E$_{(100)}$-1$_f$**	0.0	0.0	2845		109
anti-**E$_{(100)}$-1$_f$**	2.5	0.5	3029		159

[a] See Fig. 3, 5 and S2 (ESI). [b] Calculated from the *syn*/*anti* observed ratio. [c] Calculated using a cluster (Cl-1) model (See text).

In a second set of calculations, the Re···O interaction was searched between the grafted Re complex and an oxygen from silica. No such interaction could be located because the Re centre cannot approach the surface sufficiently. Therefore a surface-OH group was included in the vicinity of the grafted complex. This was done by cleaving an adjacent Si–O–Si bridge with a water molecule (**C$_{(110)hydr}$**) as shown in Fig. 7. The optimized geometries with this model show no Re···OH interaction (the Re–O$_Z$ distance remains larger than 4.9 Å).

Thus, it is clear that if such an interaction exists through for instance the presence of surface inhomogeneity, it only brings marginal extra stability to the surface complex. As a consequence, the stability of the supported catalyst cannot be attributed to this interaction. Additionally, it is also very likely that this Re···O interaction has to disappear in the course of the metathesis reaction and that the oxygen based ligand has to be replaced by the entering olefin.[63] In other words, the Re···O secondary interaction suggested by the EXAFS analysis does not modify the electronic properties of the catalyst but is evidence for the easy deformability of the rhenium fragment, which is believed to be a key factor in term of the reactivity because it prepares the catalyst to react.[63]

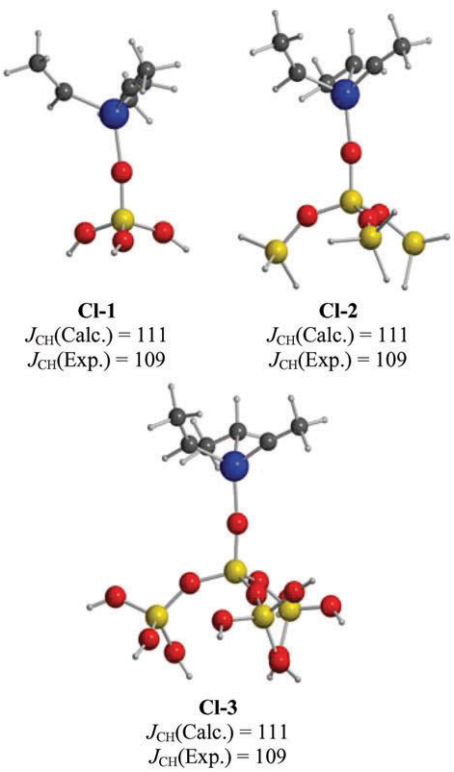

Fig. 4 NMR J_{C-H} coupling constants (Hz) for **C$_{(110)}$-1$_q$** computed using different clusters and the GAUSSIAN03 package.

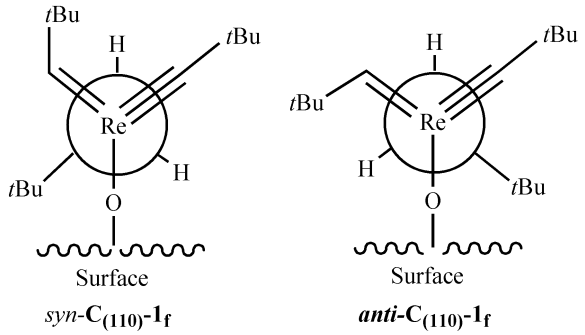

Scheme 4 Newman projections along the Re–C$_{alkyl}$ bond for the most stable conformation of *syn* and *anti* [(≡SiO)Re(≡C*t*Bu)(=CH*t*Bu)(CH$_2$*t*Bu)] isomers grafted on a cristobalite model.

Effect of the type of siloxy ligands

The optimized geometries of the *syn* and *anti* isomers of **1M$_q$** and **1P$_q$** molecular complexes are given in Fig. 2 and 8 (the structures of the full systems are presented in Figs. S1 and S3†). Tables 1 and 3 summarize the *syn*/*anti* relative energies and selected spectroscopic values for these systems. Comparing the results obtained for both *syn* and *anti* isomers of **1M$_q$** (Fig. 1) and **1P$_q$** (Fig. 8) molecular analogues with those of the models **C$_{(110)}$-1$_q$** (Fig. 3) and **E$_{(100)}$-1$_q$** (Fig. 5) of the supported system shows that they all have identical structural features around Re. The only difference is for the Si–O–Re angle whose bending is facile (very small energy differences for different SiORe angles, *vide supra*). They present the same overall tetrahedral coordination at Re with a small angle between the alkylidene and alkylidyne ligands of about 100°, the same co-planar arrangement of the alkylidene and alkylidyne ligands, the same metal to ligand bond lengths, the same

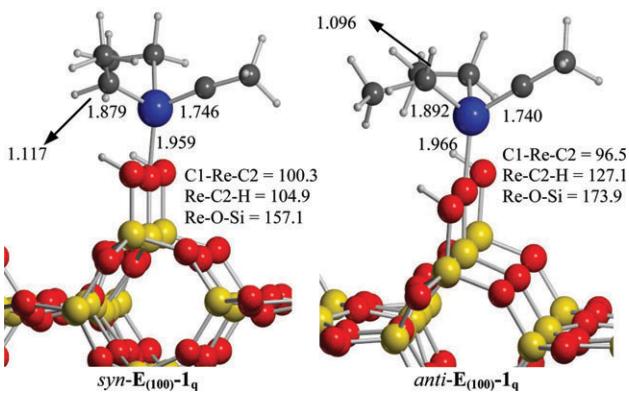

Fig. 5 Optimized structures of [(≡SiO)Re(≡CCH$_3$)(=CHCH$_3$)(CH$_2$CH$_3$)] using edingtonite as a surface model (**E$_{(100)}$-1$_q$**). See Scheme 3 for atom labelling. Distances in Å and angles in degrees.

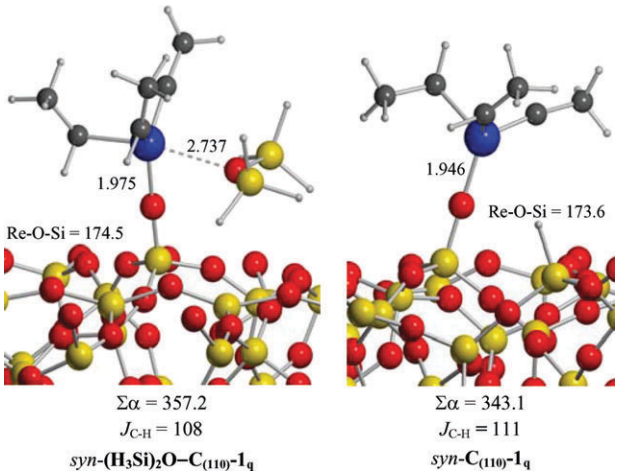

Fig. 6 Optimized structure for [(≡SiO)Re(≡CCH_3)(=$CHCH_3$)(CH_2CH_3)] in the presence of $(H_3Si)_2O$ molecule (left-hand side). The $\mathbf{C_{(110)}\text{-}1_q}$ optimized structure (right-hand side) is included for comparison. Distances in Å and angles in degrees.

alkylidene C–H bond length (1.115–1.116 Å for *syn*, 1.096 Å for *anti*) and the same differences of Re–C–H bond angles for the *syn* and the *anti* isomers (<108° for *syn*, >126° for *anti*). Moreover, the inclusion of the full set of ligands maintains the similarities between **1M**, **1P** and **1**.

The preference for the *syn* isomer is obtained in all cases. (Tables 1–3) The *anti* isomer is always close in energy, the energy difference ranging from 0.3 to 3.0 kcal mol^{-1}. In general, the surface increases slightly the preference for the *syn* isomer. The calculated stretching ν_{C-H} frequencies are marginally influenced by the nature of the siloxy group, and the frequency difference between *syn* and *anti* isomers is roughly the same (*ca.* 200 cm^{-1}) for all systems. The calculated J_{C-H} values for $\mathbf{1M_q}$ and $\mathbf{1P_q}$ are in very good agreement with experimental data (Tables 1 and 3). Therefore, comparison between the values calculated for **1M** and **1P** and those obtained for $\mathbf{C_{(110)}\text{-}1}$ and $\mathbf{E_{(100)}\text{-}1}$ shows that the nature of the siloxy ligand does not alter the spectroscopic properties of the C_{ene}–H bond.

The similarities in geometries around the rhenium centre and the equal spectroscopic values, characterizing the electronic environment of the alkylidene C–H bond in all studied

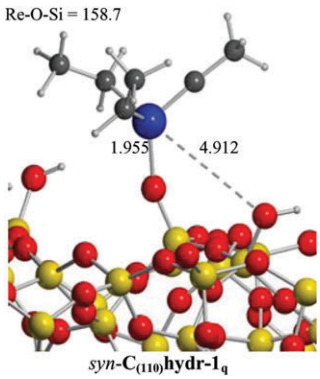

Fig. 7 Optimized structure of [(≡SiO)Re(≡CCH_3)(=$CHCH_3$)(CH_2CH_3)] in a partially hydrated cristobalite model. Distances in Å and angles in degrees.

Table 3 Relative energies in kcal mol^{-1}, stretching frequencies (ν_{C-H}) in cm^{-1} and NMR coupling constants (J_{C-H}) in Hz for C2–H bond for [$(Me)_7Si_7O_{12}SiO$–Re(≡CCH_3)(=$CHCH_3$)(CH_2CH_3)] (**$1P_q$**) and [$(Me)_7Si_7O_{12}SiO$–Re(≡C*t*Bu)(=CH *t*Bu)(CH_2*t*Bu)] (**$1P_f$**)

Structure[a]	ΔE(calc)/ kcal mol^{-1}	ΔE(exp)[b]/ kcal mol^{-1}	ν_{C-H} (calc)/cm^{-1}	J_{C-H} (calc)/Hz	J_{C-H} (exp)/Hz
syn-**$1P_q$**	0.0	0.0	2895	111[c]	116
anti-**$1P_q$**	1.5	1.4	3069	149[c]	159
syn-**$1P_f$**	0.0	0.0	2836		116
anti-**$1P_f$**	0.3	1.4	3032		159

[a] See Figs. 8 and S3 (ESI). [b] Calculated from the *syn*/*anti* observed ratio. [c] Calculated using a cluster (Cl-1) model (See text).

siloxy systems, suggest that the rhenium atom has identical electronic structure in all cases. This is further supported by an analysis of the density of states (DOS) projected on the rhenium 5d orbitals (Fig. 9). For all systems, including *syn*-$\mathbf{2M_q}$, the DOS appears as sharp peaks as expected from the molecular nature of the metal fragments even when grafted on the silica surface. There is no dispersion in the d-bands, which behave then like molecular orbitals, and will therefore be called orbitals. Although rhenium is formally a d^0 metal centre, an important d-contribution of Re orbitals is observed both in the orbitals below and above the Fermi level. For *syn*-[(X_3SiO)Re(≡CR)(=CHR)(CH_2R)] species (Fig. 9a), four orbitals with significant metal d contribution are present below the Fermi level, the three higher in energy being associated with the Re–C π-bonds (Fig. S4†). The energy and the rhenium contribution for these four orbitals are essentially identical for the molecular systems, *syn*-$\mathbf{1M_q}$ and *syn*-$\mathbf{1P_q}$, and the grafted species *syn*-$\mathbf{C_{(110)}\text{-}1_q}$ as shown in Fig. 9a. The same situation is observed for the lowest empty bands: they appear at similar energies, and they have similar metal contributions. Overall, all orbitals with significant rhenium 5d metal contribution appear at almost the same energy and with similar

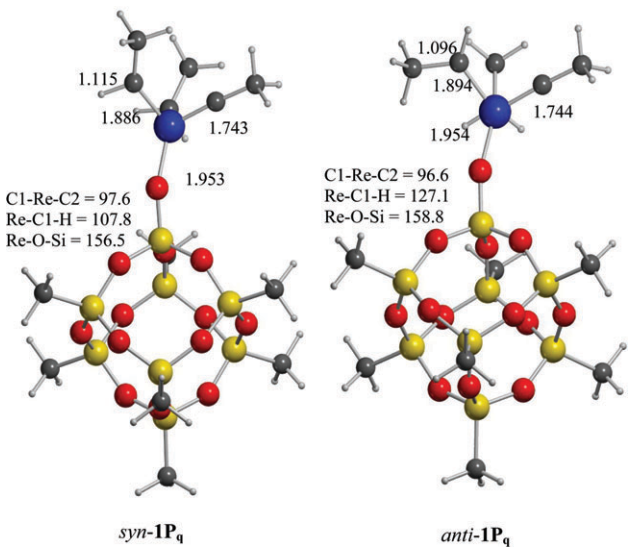

Fig. 8 Optimized structures of [$(Me)_7Si_7O_{12}SiO$–Re(≡CCH_3)(=$CHCH_3$)(CH_2CH_3)] (**$1P_q$**) computed as a periodic array of molecules with VASP package. See Scheme 3 for atom labelling. Distances in Å and angles in degrees.

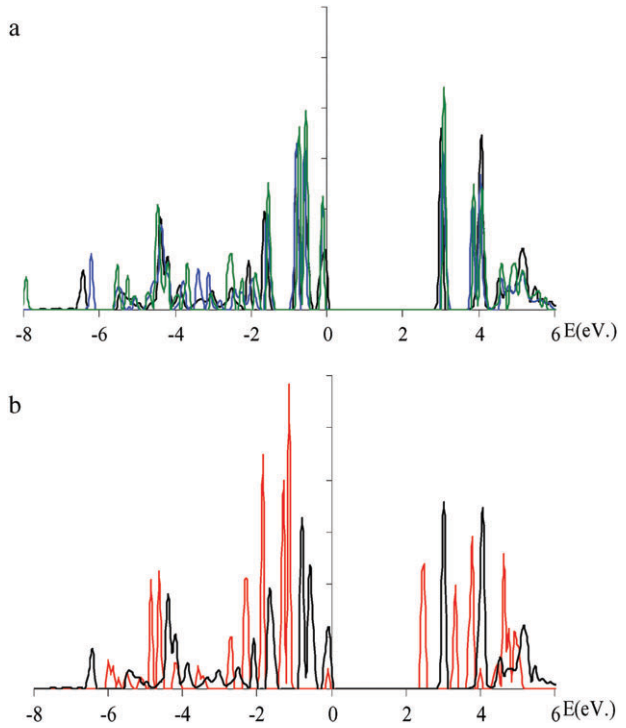

Fig. 9 DOS curves (in eV) projected to Re d orbitals for (a) ***syn*-1M$_q$** (green), ***syn*-1P$_q$** (blue) ***syn*-C$_{(110)}$-1$_q$** (black) and (b) ***syn*-2M$_q$** (red) and ***syn*-C$_{(110)}$-1$_q$** (black). The Fermi level of each system is used as the origin for energies.

metal weights, which indicates that the electronic structure around the rhenium centre is very close for *syn*-**1M$_q$**, *syn*-**1P$_q$** and *syn*-**C(110)-1$_q$**.

It is thus of interest to compare the DOS of the siloxy and the molecular bis-alkyl species, *syn*-Re(≡CCH$_3$)(=CHCH$_3$)(CH$_2$CH$_3$)$_2$ (*syn*-**2M$_q$**) (Fig. 9b). The DOS has the same number of metal based orbitals around the Fermi level, but the rhenium contribution to these orbitals as well as the energy gap between all orbitals is different from those found in the siloxy systems. The weight of Re in the occupied orbitals for *syn*-**2M$_q$** is higher than for the siloxy systems. Similarly, the empty orbitals in *syn*-**1M$_q$**, *syn*-**1P$_q$** and *syn*-**C(110)-1$_q$** have a higher contribution of Re 5d orbitals. Since there is formally no d electron on the metal centre for any of these systems, the metal contribution in the occupied bands comes only from mixing ligand and metal 5d orbitals. Because carbon is less electronegative than oxygen, its atomic orbitals are closer in energy to those of the metal, hence the metal contribution is larger in the occupied bands of bis-alkyl **2M$_q$** than in the siloxy species **1**. These results also account for the more ionic metal–ligand interactions as revealed by the NBO analysis on homologous molecular systems.[16]

From all these results on molecular species with one siloxy group, molecular species grafted on a cage with a well-defined number of SiO_2 groups and molecular species grafted on an infinite silica surface, only one conclusion can be drawn: the number of SiO_2 groups in the siloxy type ligand has no influence on the rhenium structural and electronic properties. One siloxy group acts almost as a silica surface, which indicates that the siloxy group of the first coordination sphere of the metal determines the electronic environment at Re. The only noticeable difference is the slightly more accentuated preference for the *syn* isomer in the case for the grafted species. This is associated with a larger steric repulsion between the surface and alkylidene substituents, which point toward the surface, in the *anti* isomer. In other words, the surface acts as a large siloxy ligand.

Conclusions

Plane wave periodic DFT calculations of models of the Re-based olefin metathesis catalyst, [(≡SiO)Re(≡C*t*Bu)(=CH*t*Bu)(CH$_2$*t*Bu)], show that the coordination around Re (distorted tetrahedron and metal–ligand distances for the first coordination sphere around Re) is not much affected by the nature of the siloxy group, from the simplest $OSiH_3$ to the more elaborate polyoligomeric silsesquioxane or even for a slab of silica (cristobalite or edingtonite). The experimental characteristic data for the key alkylidene group are well reproduced and nearly identical in all calculated molecular and surface systems. In the *syn* isomers, the alkylidene C–H bond is relatively long (about 1.12 Å) and the Re–C–H angle is small (about 105°), suggesting a C–H α-agostic interaction, which is also evidenced by the calculated low ν_{C-H} frequencies and low J_{C-H} coupling constants. In the *anti* isomer, all calculated data are consistent with the absence of an α-agostic C–H bond. In all systems, there is a small energy preference for the *syn* isomer by less than 3 kcal mol^{-1} as observed experimentally. Consequently, the surface siloxy groups of silica can be considered as a large siloxy ligand.[64,65]

The secondary interaction between the metal and a remote O from the surface, suggested from EXAFS measurement, does not stabilize the Re fragment and thus cannot be responsible for the stability of the surface complex. However, the Re···O secondary interaction, even if it does not lower the total energy, changes significantly the coordination at Re by turning on a new coordination site. This is additional proof of the ease of distortion of the rhenium fragment, which has been found to be a key for the high reactivity of the surface rhenium complex.

From this study, the major differences between homogeneous and surface catalysts are not associated with the intrinsic electronic difference between molecular and surface siloxy ligands. Although the transition states for olefin metathesis may be more sensitive to the nature of the siloxy ligand (molecular or surface), the higher reactivity of [(≡SiO)Re(≡C*t*Bu)(=CH*t*Bu)(CH$_2$*t*Bu)] is more likely due to the stabilization of highly reactive intermediates through site isolation, avoiding dimerization pathways, as recently suggested experimentally for isoelectronic Mo imido complexes.[66,67]

Acknowledgements

The IDRIS (grant 051744) and CINES (grant lsd2217) French national computing centers are acknowledged for a generous donation of computational time. XSM also thanks the CNRS for a post-doctoral position and Piero Ugliengo (Torino) for extremely helpful discussion.

References

1 R. L. Banks and G. C. Bailey, *Ind. Eng. Chem. Prod. Res. Dev.*, 1964, **3**, 170–173.
2 E. J. Howman and L. Turner in *Netherlands Patent Application*, British Petroleum Co. Ltd., Nl Pat. 6605328, 1966, pp. 6.
3 J. L. Hérrisson and Y. Chauvin, *Makromol. Chem.*, 1971, **141**, 161.
4 D. Astruc, *New J. Chem.*, 2005, **29**, 42–56.
5 R. R. Schrock, *Top. Organomet. Chem.*, 1998, **1**, 1–36.
6 R. R. Schrock, *J. Mol. Catal. A: Chem.*, 2004, **213**, 21–30.
7 R. H. Grubbs and S. Chang, *Tetrahedron*, 1998, **54**, 4413–4450.
8 A. Fürstner, *Angew. Chem., Int. Ed.*, 2000, **39**, 3012–3043.
9 M. R. Buchmeiser, *Chem. Rev.*, 2000, **100**, 1565–1604.
10 C. Copéret, M. Chabanas, R. Petroff Saint-Arroman and J.-M. Basset, *Angew. Chem., Int. Ed.*, 2003, **42**, 156–181.
11 C. Copéret, *New J. Chem.*, 2004, **28**, 1–10.
12 M. Chabanas, C. Copéret and J.-M. Basset, *Chem.-Eur. J.*, 2003, **9**, 971–975.
13 M. Chabanas, A. Baudouin, C. Copéret and J.-M. Basset, *J. Am. Chem. Soc.*, 2001, **123**, 2062–2063.
14 M. Chabanas, A. Baudouin, C. Copéret, J.-M. Basset, W. Lukens, A. Lesage, S. Hediger and L. Emsley, *J. Am. Chem. Soc.*, 2003, **125**, 492–504.
15 A. Lesage, L. Emsley, M. Chabanas, C. Copéret and J.-M. Basset, *Angew. Chem., Int. Ed.*, 2002, **41**, 4535–4538.
16 X. Solans-Monfort, E. Clot, C. Copéret and O. Eisenstein, *Organometallics*, 2005, **24**, 1586–1597.
17 M. Brookhart and M. L. H. Green, *J. Org. Chem.*, 1983, **250**, 395–408.
18 E. Clot and O. Eisenstein, in *Principles and Applications of Density Functional Theory in Inorganic Chemistry II*, ed. N. Kaltsoyannis and J. E. McGrady, Springer-Verlag, Heidelberg, 2004, vol. 113, pp. 1–36.
19 E. R. Davidson, *Chem. Rev.*, 2000, **100**, 351 and all articles in this issue.
20 E. Chagarov, A. A. Demkov and J. B. Adams, *Phys. Rev. B: Condens. Matter*, 2005, **71**, 075417.
21 S. Iarlori, D. Ceresoli, M. Bernasconi, D. Donadio and M. Parrinello, *J. Phys. Chem. B*, 2001, **105**, 8007–8013.
22 J. J. Mortensen and M. Parrinello, *J. Phys. Chem. B*, 2000, **104**, 2901–2907.
23 F. Vigné-Maeder and P. Sautet, *J. Phys. Chem. B*, 1997, **101**, 8197–8203.
24 M. Wallin, H. Grönbeck, A. Lloyd Spetz and M. Skoglundh, *Appl. Surf. Sci.*, 2004, **235**, 487–500.
25 I. Baraille, M. Loudet, S. Lacombe, H. Cardy and C. Pisani, *J. Mol. Struct. (THEOCHEM)*, 2003, **620**, 291–300.
26 B. Civalleri, S. Casassa, E. Garrone, C. Pisani and P. Ugliengo, *J. Phys. Chem. B*, 1999, **103**, 2165–2171.
27 S. Tosoni, F. Pascale, P. Ugliengo, R. Orlando, V. R. Saunders and R. Dovesi, *Mol. Phys.*, 2005, **103**, 2549–2558.
28 A. Del Vitto, G. Pacchioni, K. H. Lim, N. Rösch, J.-M. Antonietti, M. Michalski, U. Heiz and H. Jones, *J. Phys. Chem. B*, 2005, **109**, 19876–19884.
29 B. Griffe, A. Sierraalta, F. Ruette and J. L. Brito, *J. Mol. Struct. (THEOCHEM)*, 2003, **625**, 59–70.
30 N. López, F. Illas and G. Pacchioni, *J. Mol. Catal. A: Chem.*, 2001, **170**, 175–186.
31 R. Z. Khaliullin and A. T. Bell, *J. Phys. Chem. B*, 2002, **106**, 7832–7838.
32 Ø. Espelid and K. J. Børve, *J. Catal.*, 2000, **195**, 125–139.
33 S. Lillehaug, K. J. Børve, M. Sierka and J. Sauer, *J. Phys. Org. Chem.*, 2004, **17**, 990–1006.
34 C. Thieuleux, E. A. Quadrelli, J.-M. Basset, J. Döbler and J. Sauer, *Chem. Commun.*, 2004, 1729–1731.
35 D. V. Besedin, L. Y. Ustynyuk, Y. A. Ustynyuk and V. V. Lunin, *Top. Catal.*, 2005, **32**, 47–60.
36 M. N. Mikhailov and L. M. Kustov, *Russ. Chem. Bull., Int. Ed.*, 2005, **54**, 300–311.
37 P. Pietrzyk, *J. Phys. Chem. B*, 2005, **109**, 10291–10303.
38 L. Y. Ustynyuk, Y. A. Ustynyuk, D. N. Laikov and V. V. Lunin, *Russ. Chem. Bull., Int. Ed.*, 2001, **50**, 2050–2053.
39 M. N. Mikhailov, A. A. Bagatur'yants and L. M. Kustov, *Russ. Chem. Bull., Int. Ed.*, 2003, **52**, 30–35.
40 C. Copéret, A. Grouiller, J.-M. Basset and H. Chermette, *ChemPhysChem*, 2003, **4**, 608–611.
41 J.-M. Antonietti, M. Michalski, U. Heiz, H. Jones, K. H. Lim, N. Rösch, A. Del Vitto and G. Pacchioni, *Phys. Rev. Lett.*, 2005, **94**, 213402.
42 J. Handzlik, *J. Phys. Chem. B*, 2005, **109**, 20794–20804.
43 P. E. Blöchl, *Phys. Rev. B: Condens. Matter*, 1994, **50**, 17953–17977.
44 G. Kresse and D. Joubert, *Phys. Rev. B: Condens. Matter*, 1999, **59**, 1758–1775.
45 G. Kresse and J. Furthmüller, *Phys. Rev. B: Condens. Matter*, 1996, **54**, 11169–11186.
46 G. Kresse and J. Furthmüller, *Comput. Mater. Sci.*, 1996, **6**, 15–50.
47 J. P. Perdew, K. Burke and M. Ernzerhof, *Phys. Rev. Lett.*, 1996, **77**, 3865–3868.
48 A. H. MacDonald, *Phys. Rev. B: Condens. Matter*, 1978, **18**, 5897–5899.
49 M. J. Frisch, G. W. Trucks, H. B. Sclegel, G. E. Scuseria, M. A. Robb, J. R. Cheeseman, A. J. Montgomery, Jr, T. Vreven, K. N. Kudin, J. C. Burant, J. M. Millam, S. S. Iyengar, J. Tomasi, V. Barone, B. Mennucci, M. Cossi, G. Scalmani, N. Rega, G. A. Petersson, H. Nakatsuji, M. Hada, M. Ehara, K. Toyota, R. Fukuda, J. Hasegawa, M. Ishida, T. Nakajima, Y. Honda, O. Kitao, H. Nakai, M. Klene, X. Li, J. E. Knox, H. P. Hratchian, J. B. Cross, C. Adamo, J. Jaramillo, R. Gomperts, R. E. Stratmann, O. Yazyev, A. J. Austin, R. Cammi, C. Pomelli, J. W. Ochterski, P. Y. Ayala, K. Morokuma, G. A. Voth, P. Salvador, J. J. Dannenberg, V. G. Zakrzewski, S. Dapprich, A. D. Daniels, M. C. Strain, O. Farkas, D. K. Malick, A. D. Rabuck, K. Raghavachari, J. B. Foresman, J. V. Ortiz, Q. Cui, A. G. Baboul, S. Clifford, J. Cioslowski, B. B. Stefanov, G. Liu, A. Liashenko, P. Piskorz, I. Komaromi, R. L. Martin, D. J. Fox, T. Keith, M. A. Al-Laham, C. Y. Peng, A. Nanayakkara, M. Challacombe, P. M. W. Gill, B. Johnson, W. Chen, M. W. Wong, C. Gonzalez and J. A. Pople, *GAUSSIAN 03*, 2004, Gaussian Inc., Wallingford, CT.
50 D. Andrae, U. Häussermann, M. Dolg, H. Stoll and H. Preuss, *Theor. Chim. Acta*, 1990, **77**, 123–141.
51 A. Bergner, M. Dolg, W. Küchle, H. Stoll and H. Preuss, *Mol. Phys.*, 1993, **80**, 1431–1441.
52 A. W. Ehlers, M. Böhme, S. Dapprich, A. Gobbi, A. Höllwarth, V. Jonas, K. F. Köhler, R. Stegmann, A. Veldkamp and G. Frenking, *Chem. Phys. Lett.*, 1993, **208**, 111–114.
53 A. Höllwarth, M. Böhme, S. Dapprich, A. W. Ehlers, A. Gobbi, V. Jonas, K. F. Köhler, R. Stegmann, A. Veldkamp and G. Frenking, *Chem. Phys. Lett.*, 1993, **208**, 237–240.
54 W. J. Hehre, R. Ditchfield and J. A. Pople, *J. Chem. Phys.*, 1972, **56**, 2257–2261.
55 W. Kutzelnigg, U. Fleischer and M. Schindler, in *NMR Basic Principles and Progress*, ed. P. Diehl, E. Fluck, H. Günter, R. Kosfeld and J. Seelig, Springer-Verlag, Berlin, 1990, vol. 23, p. 165.
56 X. Solans-Monfort and O. Eisenstein, *Polyhedron*, 2006, **25**, 339–348.
57 J. Jaffart, M. Etienne, F. Maseras, J. E. McGrady and O. Eisenstein, *J. Am. Chem. Soc.*, 2001, **123**, 6000–6013.
58 J. Jaffart, R. Mathieu, M. Etienne, J. E. McGrady, O. Eisenstein and F. Maseras, *Chem. Commun.*, 1998, 2011–2012.
59 T. Ziegler and J. Autschbach, *Chem. Rev.*, 2005, **105**, 2695–2722.
60 J. Autschbach, *Struct. Bonding*, 2004, **112**, 1–48.
61 J. Vaara, J. Jokisaari, R. E. Wasylishen and D. L. Bryce, *Prog. Nucl. Magn. Reson. Spectrosc.*, 2002, **41**, 233–304.
62 T. Helgaker, M. Jaszuński and K. Ruud, *Chem. Rev.*, 1999, **99**, 293–352.
63 X. Solans-Monfort, E. Clot, C. Copéret and O. Eisenstein, *J. Am. Chem. Soc.*, 2005, **127**, 14015–14025.
64 D. G. H. Ballard, *Adv. Catal.*, 1973, **23**, 263–325.
65 L. Lefort, M. Chabanas, O. Maury, D. Meunier, C. Copéret, J. Thivolle-Cazat and J.-M. Basset, *J. Organomet. Chem.*, 2000, **594**, 96–100.
66 F. Blanc, C. Copéret, J. Thivolle-Cazat, J.-M. Basset, A. Lesage, L. Emsley, A. Sinha and R. R. Schrock, *Angew. Chem., Int. Ed.*, 2006, **45**, 1216–1220.
67 A. Sinha, L. P. H. Lopez, R. R. Schrock, A. S. Hock and P. Müller, *Organometallics*, 2006, **25**, 1412–1423.

